NMR Structure of a Protein Kinase C-γ Phorbol-Binding Domain and Study of Protein−Lipid Micelle Interactions[‡]

Robert X. Xu,[*,§] Tadeucz Pawelczyk,[||] Tai-He Xia,[§] and Stephen C. Brown[§,⊥]

Glaxo-Wellcome Research and Development, 5 Moore Drive, Research Triangle Park, North Carolina 27709, and Department of Clinical Biochemistry, Medical University of Gdansk, 80-211 Gdansk, Poland

Received April 9, 1997; Revised Manuscript Received June 9, 1997[⊗]

ABSTRACT: Classical protein kinase C (PKC) family members are activated by the binding of various ligands to one of several cysteine-rich domains of the enzyme. The natural agonist, diacylglycerol (DAG), and the natural product superagonist, phorbol dibutyrate (PDB), activate the enzyme to produce wide-ranging physiological effects. The second cysteine-rich (Cys2) domain of rat brain PKC-γ was expressed and labeled with ^{15}N and ^{13}C, and the solution structure was determined to high resolution using multidimensional heteronuclear NMR methods. The phorbol binding site was identified by titrating this domain with phorbol-12,13-dibutyrate (PDB) in the presence of organic cosolvents. Titrations of this domain with lipid micelles, in the absence and presence of phorbols, indicate selective broadening of some resonances. The observed behavior indicates conformational exchange between bound and free states upon protein−micelle interaction. The data also suggest that half of the domain, including the phorbol site and one of the zinc sites, is capable of inserting into membranes.

Protein kinase C (PKC)[1] is a family of serine/threonine kinases, first characterized by their *in vitro* activation by diacylglycerol (DAG), Ca^{2+}, and phospholipids (Nishizuka, 1984, 1992, 1995). On the basis of these activities, classical PKC family members are thought to be activated by signal transduction cascades triggered by DAG production, such as various tyrosine kinase and 7-transmembrane receptors which stimulate phospholipases C (Weinstein, 1988). PKC is also the major receptor mediating tumor promotion by the natural product superagonist phorbol and ingenol esters (Bell & Burns, 1991). Phorbol esters have been used extensively as pharmacological tools to investigate PKC functions *in vivo* (Sharkey et al., 1984), revealing the role of PKC in diverse inflammatory and mitogenic processes. Dissection of the various roles of PKC *in vivo* is complicated by the existence of isotypes differing in primary sequence, tissue expression patterns, subcellular localization, activation properties, and responsiveness to receptor signal mediated activation (Dekker & Parker, 1994).

Deletion analyses of the diacylglycerol and phorbol-responsive PKC-γ (Ohno et al., 1989; Quest et al., 1994a) isoform revealed two Zn-binding domains (Figure 1), labeled Cys1 and Cys2 within the first constant domain (C1), that were responsible for activation by DAG and phorbol esters. Each of these two domains, expressed as recombinant proteins, bound two mol equiv of Zn and demonstrated affinities for DAG and phorbols comparable to those of intact PKC protein (Burns & Bell, 1991; Quest et al., 1994b). Site-directed mutagenesis studies (Kazanietz et al., 1995) and an X-ray crystal structure of a PKC-δ Cys2/phorbol complex (Zhang et al., 1995) confirm that the Cys2 domain represents the domain responsible for DAG/phorbol binding and subsequent activation of PKC. However, the enzyme is activated by localization to cellular membranes subsequent to DAG/phorbol binding, where the protein is more labile as judged by proteolytic sensitivity (Burns & Bell, 1991; Newton, 1993).

Besides DAG and phorbol esters, several negatively charged lipid effectors are also capable of partial PKC activation at relatively high concentrations of Ca^{2+} (10^{-4}−10^{-3} M). However, at low Ca^{2+} concentrations (10^{-6} M), only phosphatidylserine in conjunction with DAG leads to high levels of PKC activity. Thus, phosphatidylserine (PS) is thought to represent a principal, physiologically relevent phospholipid cofactor. Stereospecific interactions between PKC and the amino, carboxyl, and phosphate moiety of the PS headgroup are critical for activation (Lee & Bell, 1989). Therefore, the interactions of other lipids, such as PS, with PKC require investigation to clarify the structural and biochemical mechanisms resulting in activation.

The structural basis of PKC activation by DAG and tumor-promoting natural product ligands has been modeled on the basis of known SAR relationships among these diverse ligands (Rando & Kishi, 1992). It is likely that superactivation by the natural products is achieved through conformational preorganization, by restricting the unbound conformational repertoire of these ligands to that binding PKC.

[‡] The coordinates of the 30 final simulated annealing structures of PKC-γ and the energy-minimized average structure have been deposited in the Brookhaven Protein Data Bank (filenames: 1TBN, energy-minimized average structure; 1TBO, 30 refined structures).

* To whom correspondence should be addressed.

[§] Glaxo-Wellcome Research and Development.

[||] Medical University of Gdansk.

[⊥] Present address: Park Davis Pharmaceutical Research, 2800 Plymouth Road, Ann Arbor, MI 48105.

[⊗] Abstract published in *Advance ACS Abstracts,* August 15, 1997.

[1] Abbreviations: PKC, protein kinase C; DAG, 1,2-diacylglycerol; SAR, structure−activity relationship; PDB, phorbol 12,13-dibutyrate; PS, 1,2-diacylphosphatidylserine; DPC, dodecylphosphocholine; NMR, nuclear magnetic resonance; ATP, adenosine 5′-triphosphate; GST, glutathione *S*-transferase; CHAPS, 3-[(3-cholamidopropyl)dimethylammonio]propanesulfonate; PBS, phosphate-buffered saline; IEF, isoelectric focusing; DTT, dithiothreitol; RF, radio frequency; HSQC, heteronuclear single-quantum coherence; TOCSY, total correlation spectroscopy; HMQC, heteronuclear multiple-quantum coherence; NOESY, nuclear Overhauser effect spectroscopy; DG, distance geometry; SA, simulated annealing; D_2O, deuterium oxide; CD_3OD, perdeuterated methanol; ESI, electrospray ionization; AOP, angular order parameter; rmsd, root mean square deviation.

S0006-2960(97)00833-7 CCC: $14.00

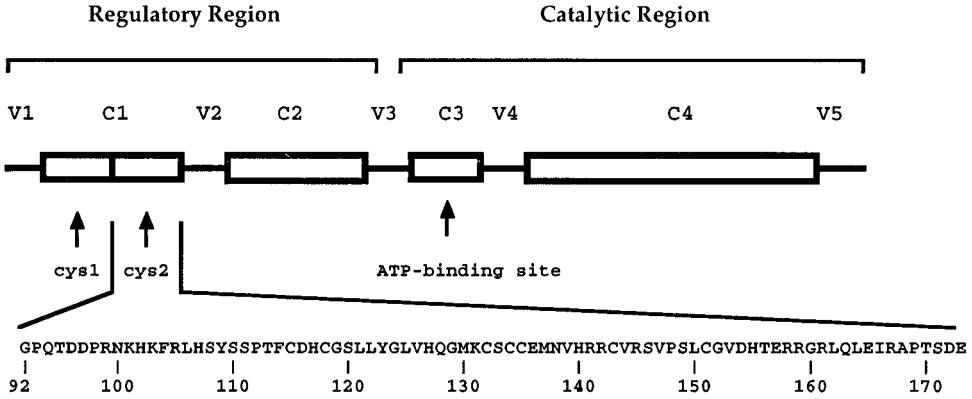

FIGURE 1: Domain structure of rat brain PKC-γ. PKC isoforms contain constant (C) and variable (V) domains located within their aligned sequences. The amino acid sequence of the Cys2 domain is shown.

This pharmacophore was verified by modeling and SAR studies (Wang et al., 1994a,b) which also revealed that hydrophobicity and conformational energy are important properties of PKC Cys2 ligands. Recently published experimental evidence indicates, however, that DAG and phorbols can bind *simultaneously* to PKC-α, complicating the discernment of their sites of interaction with the protein and each other (Slater et al., 1996). In spite of extensive screening efforts, very few *inhibitors* of PKC activation have been identified. Most discovered PKC inhibitors are directed against the PKC catalytic domain and are either ATP analogues (e.g., bisindolylmaleimides) or substrate analogues (Toullec et al., 1991; Martigny-Baron et al., 1993). Sphingosine and calphostin C are the only ligands identified to date that inhibit PKC by binding to the Cys2 domain.

Though two NMR-derived solution structures of the PKC-α Cys2 domain have been published (Hommel et al., 1994; Ichikawa et al., 1995), studies of lipid and other ligand (such as phorbols) interactions in solution with this PKC regulatory domain have not been reported to date. A high-resolution X-ray crystal structure of the PKC-δ Cys2 domain complexed with phorbol 13-acetate (Zhang et al., 1995) reveals details of the phorbol−protein interaction, but in the absence of lipids required for functional activation. Moreover, phorbol 13-acetate is not a potent activator of PKC, commensurate with the requirement of hydrophobicity in the ester side chains of phorbol derivatives for potent enzyme activation. Thus, high-resolution solution structural studies by heteronuclear multidimensional NMR methods could help to reveal the nature of PKC activation by DAG/phorbols and perhaps help to discover requirements for antagonism of PKC at the same ligand-binding site.

MATERIALS AND METHODS

Protein Expression. Escherichia coli BL21(DE3) cells were transfected with pGEM-2TKG plasmid containing the GST gene linked to the Cys2 domain of rat PKC-γ (92−173) through an extended thrombin cleavage site (Figure 1). The colonies were grown on LB agar plates containing carbenecillin. Picked colonies were grown overnight at 37 °C in LB medium, and 1 mL of this culture was inoculated into 1 L of fresh LB medium. Bacteria were weaned from LB media to M9/glucose in 100 mL overnight cultures and then seeded into 1 L cultures of M9/glucose supplemented with thiamin (10 mg/L) and $ZnSO_4$ (200 μM). $^{15}NH_4Cl$ (Cambridge Isotopes, 98%) and [^{13}C]glucose (Cambrige Isotopes, 98%) were used to uniformly label the expressed protein with either ^{15}N alone or ^{15}N and ^{13}C together. Cultures were grown at 37 °C to OD_{600} ~0.6 and then induced with IPTG while the temperature was lowered to 20 °C (Ghosh et al., 1995). Trial runs indicated that different times were required for optimal production of ^{15}N-labeled (~12 h) and ^{15}N,^{13}C-labeled (~24 h) protein.

Protein Purification. All steps were done at 4 °C. Bacterial cultures (1−10 L) were combined and cells harvested by centrifugation. The pellet from 1−5 L cultures was suspended in 40 mL of buffer A [50 mM $NaPO_4$ (pH 7.4), 150 mM NaCl, 1 mM EDTA, 10 mg/L leupeptin, 0.2 mM Pefablock SC (AEBSF), 1 mM benzamidine, 5 mM β-mercaptoethanol (βMe), 10 mM CHAPS]. Resuspended cells were French-pressed (1000 psi, high level) and then clarified by centrifugation (50000*g*, 30 min) and filtration (0.45 μm). The cleared cell lysate was passed through a 5 mL glutathione−Sepharose 4B (Pharmacia) column pre-equilibrated with buffer A; then the column was washed (buffer A supplemented with 1 mM ATP and 10 mM $MgCl_2$) until no more protein was eluting, as determined by Coomassie spot tests. The GST−Cys2 fusion protein was then eluted from the column with buffer B [50 mM $NaPO_4$, 20 mM Tris-HCl (pH 8.0), 150 mM NaCl, 30 mM glutathione (reduced)]. Fractions containing high protein content were combined and dialyzed overnight [PBS (pH 7.6), 2 mM βME, 10 μM $ZnCl_2$]. Protein content of the dialysate was estimated (1 OD_{280} ~ 0.5 mg/mL), and the Cys2 protein was cleaved from GST by thrombin digestion. Three units of thrombin (Novagen, restriction grade) was added per milligram of protein, $CaCl_2$ was added to 2.5 mM, and digestion was done at pH 7.4, 25 °C, until quantitatively complete (4−5 h). The thrombin digest was passed through a 5 mL glutathione−Sepharose 4B column to recover Cys2 protein. The major impurities at this point were glutathione and β-mercaptoethanol adducts, which were hydrolyzed during the subsequent dialysis by addition of 50 mM DTT to the dialysis bag. Pooled fractions were dialyzed overnight against 50 mM KPO_4 (pH 7.0) and then loaded onto a Mono-S (HR 5/5) column preequilibrated with the same buffer. Cys2 protein eluted at ~320 mM KCl during a 0−500 mM linear KCl gradient. This step was necessary to separate properly Zn-coordinated Cys2 from unfolded and misfolded species. Eluted pure Cys2 protein was dialyzed overnight against PBS [10 mM $NaPO_4$ (pH 6.8), 150 mM NaCl] and concentrated (Centriprep-3, Amicon). Protein purity was verified using Tricine and IEF gels (Novex) and identity confirmed by ESI mass spectrometry: $(M + H)^+ = 9358$ amu.

NMR Sample Preparation. Protein stock solutions were stored dilute (50−100 μM) under argon gas in a buffer containing 50 mM KPO_4 and 100 mM KCl (pH 6.7) at 4 °C. Immediately before use, protein stock was concentrated to the appropriate concentration using Centricon-3 (Amicon) tubes and transferred to NMR tubes. Perdeuterated DTT (Cambridge Isotope Labs) was added to 1 mM concentration, the solution was layered with argon gas, and the tube was sealed with parafilm.

NMR Spectroscopy. NMR data were collected at 20 °C on a Varian Unity−Plus 600 spectrometer equipped with a Nalorac triple resonance probehead containing a self-shielded *z*-gradient. Waveform generators were used to execute frequency-offset pulses so that only three RF channels were used for triple resonance experiments. Gradient-enhanced coherence selection was used in all triple resonance experiments (Muhandiram & Kay, 1994) as well as all other ^{15}N HSQC (Kay et al., 1992) related experiments. Gradients were also used for artifacts and solvent suppression (Bax & Pochapsky, 1992). Water flip-back methods (Kay et al. 1994) were applied to the experiments that start from amide proton magnetization. Oversampling and in-line digital filtering were used in direct acquisition for all experiments. All NMR data were processed with NMRPIPE (Delaglio et al., 1995) and analyzed with GXNMR (Xia, 1996) on a Silicon Graphics workstation. Solvent suppression filters were applied to the acquisition time domain. Mirror image linear prediction (Zhu & Bax, 1990) or forward−backward linear prediction (Zhu & Bax, 1992) was used in indirect time domains to extend data points up to twice the number of points collected, after Fourier transforms were done in all the other dimensions (Schussheim & Cowburn, 1987).

Chemical Shift Assignments. Sequential resonance assignments were accomplished using data sets from the following 3D experiments. All the following data were collected with a ^{1}H (F_3) carrier frequency of 4.82 ppm with a spectral width of 9434 Hz, a ^{15}N (F_1) carrier frequency of 120.6 ppm with a spectral width of 1582 Hz, and 16 transients. The CBCA(CO)NH (Grzesiek & Bax, 1992) and HNCACB (Wittekind & Muller, 1993) were collected with ^{13}C (F_2) spectral widths of 10 262 and 10 000 Hz centered on 46 ppm. A C(CO)NH-TOCSY (Logan et al., 1992, 1993; Grzesiek et al., 1993a) was collected with a ^{13}C (F_2) spectral width of 10 262 Hz centered on 44 ppm. The mixing time of the TOCSY was 20 ms. These three experiments provided C_α, C_β connections and possible residue types along the protein sequence (Olejniczak et al., 1992; Grzesiek & Bax, 1993a). The C_α peaks can easily be distinguished from C_β peaks on the basis of chemical shift values. In HNCACB, C_β peaks also have opposite signs from C_α peaks. Besides C_α, C_β chemical shifts, the additional carbon chemical shifts provided by C(CO)NH-TOCSY limited the possible residue types. The HBHA(CO)NH (Grzesiek & Bax, 1993a) and ^{15}N TOCSY-HSQC (Marion et al. 1989) were collected with a ^{1}H (F_2) spectral width of 6000 Hz. The mixing time of the TOCSY is 35 ms. These two experiments provided H_α, H_β connections along the protein sequence. The identified carbon and proton resonances also provide the starting points for the subsequent side-chain assignments.

The aliphatic side-chain resonances were assigned by 3D HCCH-TOCSY (Bax et al., 1990a) and HCCH-COSY (Bax et al., 1990b). Both of these data sets were collected with eight transients per FID. The ^{1}H carrier frequency was at 4.82 ppm and the ^{13}C at 43.3 ppm. The spectral widths were 6385.7 Hz for ^{1}H (F_1), 4248.1 Hz for ^{13}C (F_2), and 7806.4 Hz for ^{1}H (F_3). The mixing time of FLOPSY-8 is 20 ms.

The aromatic side-chain resonances were assigned by a modified version (B. T. Farmer, II, personal communication, 1996) of 2D CB(CGCD)HD (Yamazaki et al., 1993), 2D CB(CGCDCE)HE (Yamazaki et al., 1993), and 3D C-C-H AMNESIA (Grzesiek & Bax, 1995). A 3D HCCH-COSY was also used to confirm the assignments. The CB(CGCD)-HD data were collected with 768 transients per FID and a spectral width of 4800 Hz for ^{13}C (F_1) and 7806.4 Hz for ^{1}H (F_2). The CB(CGCDCE)HE data were collected with 512 transients per FID and a spectral width of 9600 Hz for ^{13}C (F_1) and 7806.4 Hz for ^{1}H (F_2). The 3D C-C-H AMNESIA was carried out with 64 transients and spectral widths of 5710 Hz for ^{13}C (F_1), 5000 Hz for ^{13}C (F_2), and 7806.4 Hz for ^{1}H (F_3). The 3D HCCH-COSY was carried out with 16 transients and spectral widths of 4800 Hz for ^{1}H (F_1), 4800 Hz for ^{13}C (F_2), and 7806.4 Hz for ^{1}H (F_3).

Coupling Constant Measurement and Stereospecific Assignments. The 3D ^{15}N TOCSY-HSQC was used to determine $^3J_{H\alpha-H\beta}$ using the parameters described above. A 3D HNHB data set (Archer et al., 1991) was collected to determine the $^3J_{N-H\beta}$. The spectral widths were 5400 Hz for ^{1}H (F_1), 1582 Hz for ^{15}N (F_2), and 9434 Hz for ^{1}H (F_3). The 3D HN(CO)HB (Grzesiek et al., 1992) data was acquired to measure $^3J_{CO-H\beta}$. using spectral widths the same as for the 3D HNHB experiment. From these three coupling constants, the χ^1 angle and stereospecific assignments for some of the β-methylene protons were determined.

The HMQC-*J* (Kay & Bax, 1990) and 3D HNHA (Vuister & Bax, 1993a) data were collected to measure the $^3J_{HN-H\alpha}$. The ϕ angle was set to $-120 \pm 30°$ when $^3J_{HN-H\alpha} > 9$ Hz. The stereo-specific assignments and the dihedral angles of χ^2, χ^3, and χ^1 for methyls were determined on the basis of the following coupling constant measurements. The 3D long-range C−C (Bax et al., 1992) was used to determine $^3J_{C\delta-C'}$ in Leu and Ile and $^3J_{C\gamma-C'}$ in Val, Thr, and Ile, as well as $^3J_{C\epsilon-C\beta}$ in Met. The spectral widths were 2565 Hz for ^{13}C (F_1), 12 987 Hz for ^{13}C (F_2), and 7994 Hz for ^{1}H (F_3). The ^{13}C carrier was at 37 ppm. The 3D long-range C−H (Vuister & Bax, 1993b) was collected to determine $^3J_{C\delta-H\beta}$ in Leu and Ile and $^3J_{C\gamma-H\alpha}$ in Val, Thr, and Ile. The spectral widths were 2273 Hz for ^{13}C (F_1) centered at 18.7 ppm, 2689 Hz for ^{1}H (F_2), and 7240 Hz for ^{1}H (F_3) centered at 1.64 ppm. The difference data set of 2D constant time ^{13}C HSQC with/without ^{13}C═O (Grzesiek et al., 1993b) or ^{15}N coupling (Vuister et al., 1993a) was acquired to measure $^3J_{C\gamma-C'}$ or $^3J_{C\gamma-N}$ in Val, Thr, Ile, and Lys. The spectral widths of the 2D data were 4980 Hz for ^{13}C for (F_1) centered at 24.6 ppm and 7189 Hz for ^{1}H (F_2) centered at 4.82 ppm.

*Interproton Distance*s. The 3D ^{15}N NOESY-HSQC (Fesik & Zuiderweg, 1988; Zhang et al., 1994) with a mixing time of 150 ms was collected. The spectral widths were 7000 Hz for ^{1}H (F_1), 1582 Hz for ^{15}N (F_2), and 9434 Hz for ^{1}H (F_3). The 4D ^{13}C/^{13}C HMQC-NOESY-HSQC (Vuister et al., 1993b) with a mixing time of 90 ms was recorded with $10 \times 66 \times 10 \times 512$ complex points. To maintain sensitivity, eight transients were accumulated for each FID, giving a total measuring time of 6 days. The spectral widths were 3290 Hz for ^{13}C (F_1), 5401 Hz for ^{1}H (F_2), 3290 Hz for ^{13}C (F_3), and 7189 Hz for ^{1}H (F_4). The data were Fourier transformed in the order of the t_1, t_4, and t_2 dimension before mirror image linear prediction doubled the points in t_3. The F_2 and F_1 were then inverse Fourier transformed and mirror

Table 1: Structural Statistics and rmsd for the 30 PKC-γ Structures[a]

structural statistics	⟨SA⟩	$(\overline{SA})_r$
rmsd (Å) from exptl distance restraints (696)	0.0096 ± 0.0018	0.0081
rmsd (deg) from exptl dihedral angle restraints (95)	0.252 ± 0.048	0.215
X-PLOR energies (kcal/mol)		
E_{tot}[b]	96.8 ± 3.5	91.4
E_{bond}	4.0 ± 0.2	3.6
E_{angle}	78.8 ± 1.6	76.5
E_{impr}	8.1 ± 0.5	7.3
E_{repel}[c]	2.2 ± 0.6	1.4
E_{cdih}[d]	0.38 ± 0.14	0.27
$E_{NO}E$[d]	3.3 ± 1.2	2.3
$E_{L\text{-}J}$[e]	−163 ± 19	−161
deviations from idealized covalent geometry		
bonds (Å)	0.002 ± 0.000	0.002
angles (deg)	1.436 ± 0.148	1.278
impropers (deg)	0.518 ± 0.156	0.365

Cartesian coordinate rmsd (Å) ⟨SA⟩ vs (SA)	N, C_α, C′	all non-H
residues 100−153	0.50 ± 0.09	1.10 ± 0.15
ordered structure[f]	0.34 ± 0.07	0.98 ± 0.13

[a] ⟨SA⟩ is the ensemble of the 30 final simulated annealing structures. (SA) is the mean structure obtained by averaging the coordinates of the 30 SA structures best fit to each other, and $(\overline{SA})_r$ is the energy-minimized structure. [b] The total energy E_{tot} does not include Lennard-Jones van der Waals energy. [c] The value of the quartic van der Waals repulsion term E_{repel} is calculated with a force constant of 4 kcal·mol^{-1}·Å^{-4}, with the van der Waals hard sphere radii set to 0.75 times those in the X-PLOR parameter set. [d] The E_{cdih} and E_{NOE} were calculated using force constants of 200 kcal·mol^{-1}·rad^{-2} and 50 kcal·mol^{-1}·Å^{-2}, respectively. [e] The Lennard-Jones van der Waals energy is not included in the target function for simulated annealing. [f] The ordered structure includes all the secondary structures and well-defined turns (102−108, 112−122, and 129−147).

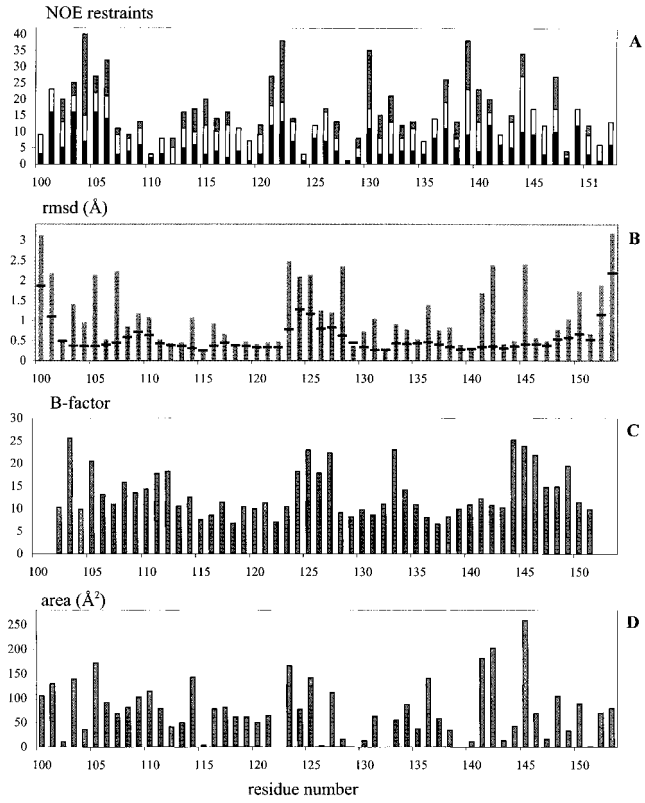

FIGURE 2: (A) Distribution of restraints from NOE data by residue. The solid bars are the intraresidue restraints, the clear bars are sequential ($|i - j| = 1$) and short-range ($2 < |i - j| \leq 5$) restraints, and the gray bars are the long-range ($|i - j| > 5$) restraints. The total number of restraints for each residue is represented by the stack height. (B) rmsd by residue from 30 NMR-derived solution structures. The gray bar heights and the small solid rectangle levels represent the rmsd to the mean atomic coordinates for all the non-hydrogen side-chain atoms and the backbone N, Cα, and C′ atoms, respectively. (C) *B*-factors from the X-ray derived structure (Zhang et al., 1995). (D) The solvent-accessible surface area (Å) for the energy-minimized mean structure. The probe radius is 1.6 Å. For clarity, only residues 100−153 are displayed.

image linear predicted to double the points in the t_2 and t_1 domains (Clore et al., 1991). Hyperbolic secant inversion pulses (420 ms) (Silver et al., 1984) were used to improve inversion quality on carbon. Although the ^{13}C carrier frequency was at 43.7 ppm, most of the aromatic−aliphatic NOE cross-peaks found in the 3D ^{13}C NOESY spectrum can be identified in the 4D data set. To maximize the number of aromatic−aliphatic NOEs found, a 3D ^{13}C NOESY-HSQC (Muhandiram et al., 1993) data set was collected with ^{13}C carrier at 78 ppm. A hyperbolic secant inversion pulse was also used in the HSQC part of this experiment. The STUD (Bendall & Skinner, 1996) decoupling scheme was used for ^{13}C decoupling in the acquisition. The spectral widths were 7000 Hz ^{1}H (F_1), 4248 Hz for ^{13}C (F_2), and 7205 Hz for ^{1}H (F_3). Volumes of the NOE cross-peaks were corrected for relaxation and transfer efficiencies (Meadows et al., 1993). The distance restraints of fixed distances (e.g., distances between geminal protons or vicinal ring protons) were excluded from the structure calculations. When a third proton has NOEs with both geminal protons, the spin diffusion between geminal protons reduces the intensity of the shorter distance NOE and enhances the intensity of the longer distance NOE. If a third proton has distance restraints to both stereospecifically assigned geminal protons, the longer one was ignored in the structure calculation to avoid distance restraint violation.

Hydrogen Bond Restraints. The hydrogen bond restraints were deduced on the basis of slowly exchanging amide protons and the pattern of sequential and interstrand NOEs involving HN and H_α (Wuthrich, 1986). The HN exchange rates and NOEs with water were measured by 2D water-ROESY and 2D water-NOESY (Grzesiek & Bax, 1993b).

Structural Restraints. A total of 664 unique interproton distances, which included 373 intraresidue (56.2%), 138 sequential (20.8%), 37 short-range (2−5 residues apart) (5.6%), and 116 long-range (>5 residues apart) (17.5%) restraints were used in the structure calculation. A total of 51 ϕ, 2 ψ, 37 χ^1, 4 χ^2, and 1 χ^3 angle restraints were used in the structure calculation. There were 16 hydrogen donor−acceptor pairs identified from the data, and these were included as 32 distance restraints using X-PLOR parameters H → O (1.8−2.3 Å) and O → N (2.5−3.3 Å).

Structure Calculations. Distance geometry (DG) and simulated annealing (SA) (Nilges, 1988) were used with X-PLOR 3.1 (Brunger, 1992) installed on a four-processor Silicon Graphics Challenge computer. Because of the lack of distance restraints at N- and C-termini, only residues 94−159 were included in the calculation. An initial 250 DG embedded substructures were refined by the SA procedure as described previously (Xu et al., 1995). The initially refined structures were calculated without Zn atoms. The Zn-binding sites of the initially refined structures were carefully examined to see if the NOE assignments consistently hold Zn-binding sites within bond distance. This strategy avoided the possible bias that might be introduced by Zn−protein bonds. The Zn atoms were then added to

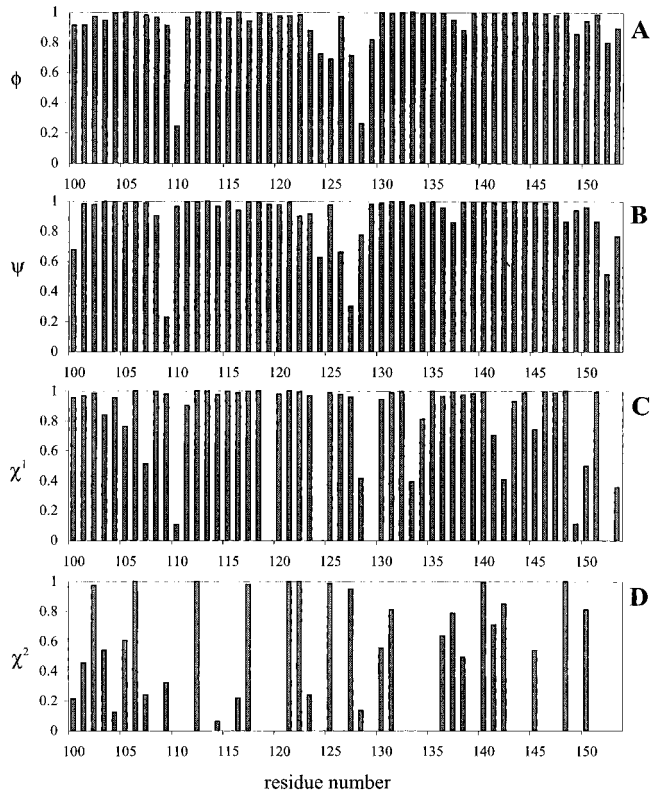

FIGURE 3: Angular order parameter (AOP) by residue for the backbone ϕ (A) and ψ (B) and the side-chain χ^1 (C) and χ^2 (D) angles for the 30 NMR solution structures. No deviation in a specified dihedral angle will produce an AOP = 1.0. Rotations about χ^2 bonds in residues with symmetrically branched side chains may lead to an reduction of the order parameter (Meadows et al., 1993). For clarity, only residues 100−153 are displayed.

the later structure calculations with covalent bonds to the Nδ^1 (2.0 Å) of the histidine and Sγ (2.3 Å) of the cysteine residues.

Phorbol/Lipid Titrations. Phorbol derivatives (Sigma), pure lipids (Avanti Polar Lipids), and deuterated lipids (Avanti, Cambridge Isotope Labs) were purchased and used fresh for all titrations. Phorbol 12,13-dibutyrate, 4β-phorbol, phorbol 13-acetate, 4α-phorbol, $(8:0)_2$-diacylglycerol, $(14:0)_2$-diacylglycerol, $(8:0)_2$-phosphatidylserine, $(14:0)_2$-phosphatidylserine, $(18:1)_2$-phosphatidylserine, $(14:0)_2$-phosphatidylserine-d_{54}, $(14:0)_2$-phosphatidylcholine, $(18:1)_2$-phosphatidylcholine, and dodecylphosphocholine-d_{38} were made up as concentrated stock solutions (10−100 mM) in either D_2O, CD_3OD, or $CDCl_3$. Purity and structure of all lipids were verified by ESI mass spectrometry and NMR of stock solutions, which were stored at 4 °C in NMR tubes. Aliquots for titrations were taken directly from stock solutions, or they were pipetted into glass Reacti-Vials (Pierce), the solvent was evaporated by either a dry nitrogen gas stream or lyophilization, and the resulting solids were dissolved into the solution of interest. Phorbols are highly inflammatory natural products and must not contact skin, eyes, or other body surfaces. Therefore, all solutions containing phorbols were handled carefully with gloves, and the phorbols were destroyed by 10 N NaOH when experiments were finished. Lipids having shorter acyl chains (n < 12), such as DPC, PDB, and $(8:0)_2$DAG, were generally cosoluble and present as mixed micelles, while lipids having longer fatty acyl chains, such as $(18:1)_2$-phosphatidylserine, could be incorporated at low mole fractions within micelles of shorter acyl chain lipids. Some mixed micelles were, however, unstable over time and aggregated after several hours. Lipid micelles of various compositions were generally clarified by brief sonication of deaerated solutions under argon gas. Survey titrations were generally done at 100 μM protein, with lipid concentrations reported as ratios to the protein concentration. All titrations were replicated from all possible different starting points, to cover the entire range of proportions and ensure proper end-point determinations.

RESULTS AND DISCUSSION

Quality of the NMR Solution Structures. Thirty low-energy structures were selected from 250 DGSA structures. The statistics for the final structures are outlined in Table 1. The low deviation from idealized covalent geometry, low X-PLOR energies, and negative $E_{L\text{-}J}$ term reflected the good

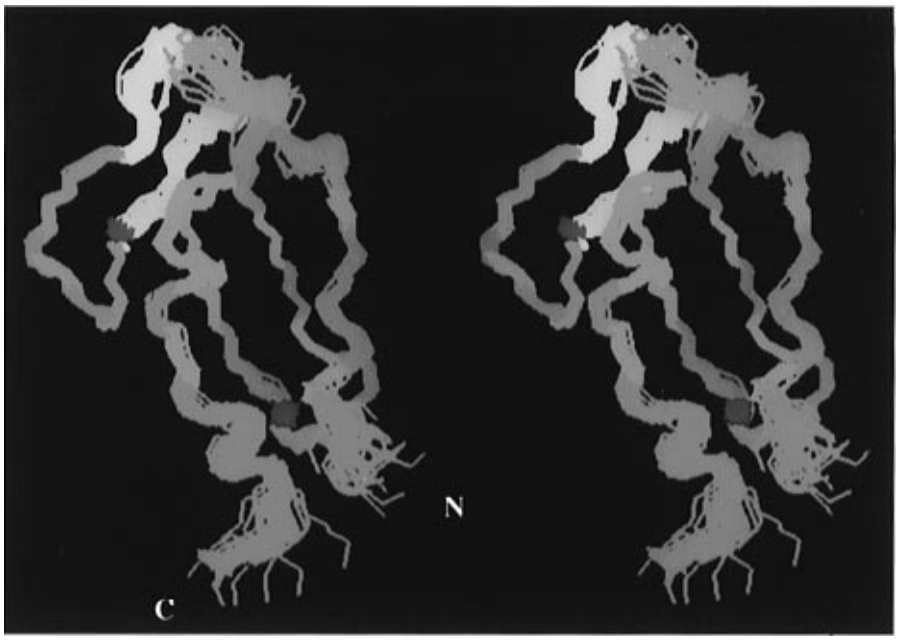

FIGURE 4: Superimposed stereoview of the 30 NMR solution structures of the PKC-γ Cys2 domain. The zinc atoms are colored red. The PDB interacting residues are colored yellow. The residues whose amide signals of the ^{15}N HSQC spectrum became broadened upon lipid binding, in the absance of phorbol, are colored cyan. For clarity, only residues 100−153 are displayed.

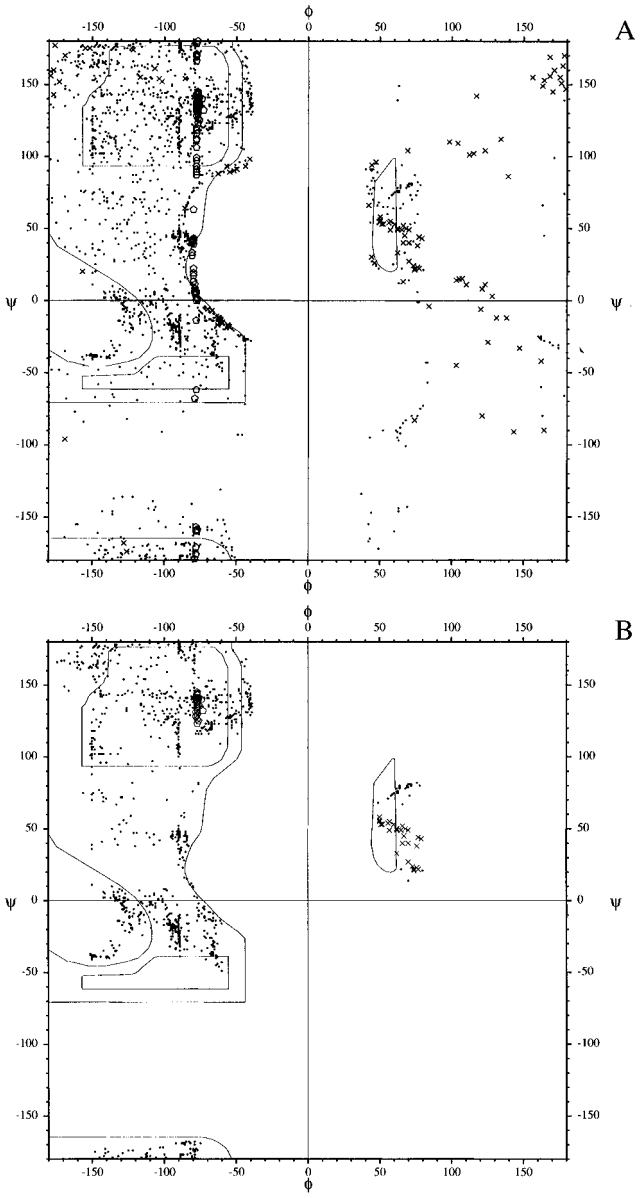

FIGURE 5: (A) Ramachandran plots for all the ϕ and ψ angles in the 30 NMR structures of PKC-γ Cys2. (B) Only those residues with ϕ and ψ AOP values >0.9.

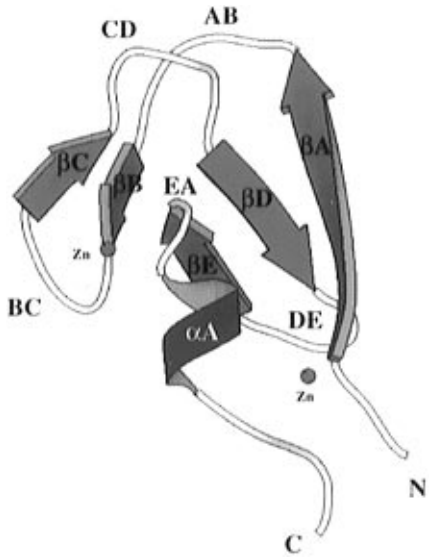

FIGURE 6: Ribbon diagram of the secondary structure of PKC-γ Cys2. The figure was generated with the program Molscript (Kraulis, 1991).

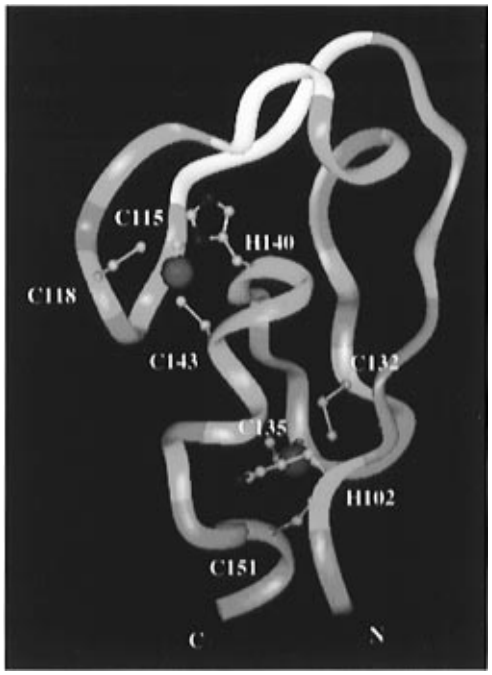

FIGURE 7: The Solid_Oval diagram is calculated from the backbone of the energy-minimized mean structure of PKC-γ Cys2. The zinc atoms are big red balls. The zinc-binding side chains are small ball and stick models with carbon in gray, nitrogen in blue, and sulfur in yellow. The phorbol-binding residues are in yellow, and the residues broadened upon binding of lipid micelles, in the absence of phorbol, are colored cyan. For clarity, only residues 100−153 are displayed.

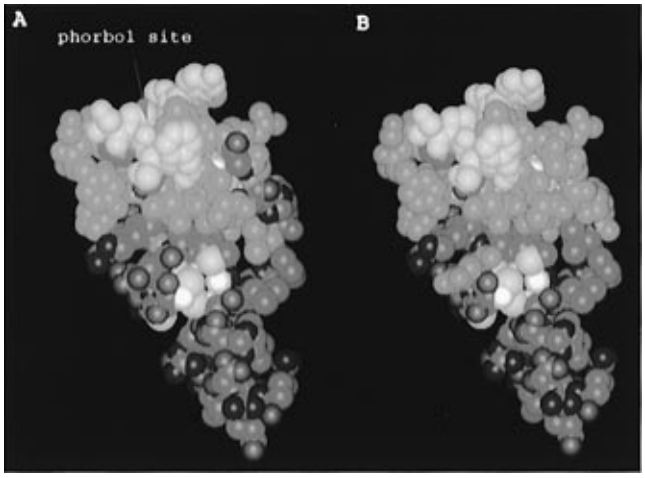

FIGURE 8: van der Waals surface generated with INSIGHT from the energy-minimized mean structure of PKC-γ Cys2 (coloring as in Figure 7). The residue signals of the ^{15}N HSQC that were broadened upon binding of lipid micelles are colored cyan (A) in the absence of phorbol and (B) in the presence of phorbol. Residues that were included in the structure calculation (94−159) are displayed.

quality of the structures. No distance restraint violation was greater than 0.2 Å and no dihedral angle restraint violation was more than 3°. In the intermediate refined structures without Zn atoms, the distance restraints from NOE consistently hold Zn-binding sites within bond distance. The N-terminal residues before N100 are very flexible, as are the residues after V153 at the C-terminus. Therefore only residues 94−159 were included in structure calculations. The rmsd for the backbone and all heavy atoms in each residue are presented in Figure 2. A plot for the angular order parameter (AOP) of the ϕ, ψ, χ^1, and χ^2 angles is presented in Figure 3. The rmsd about the mean coordinates for the

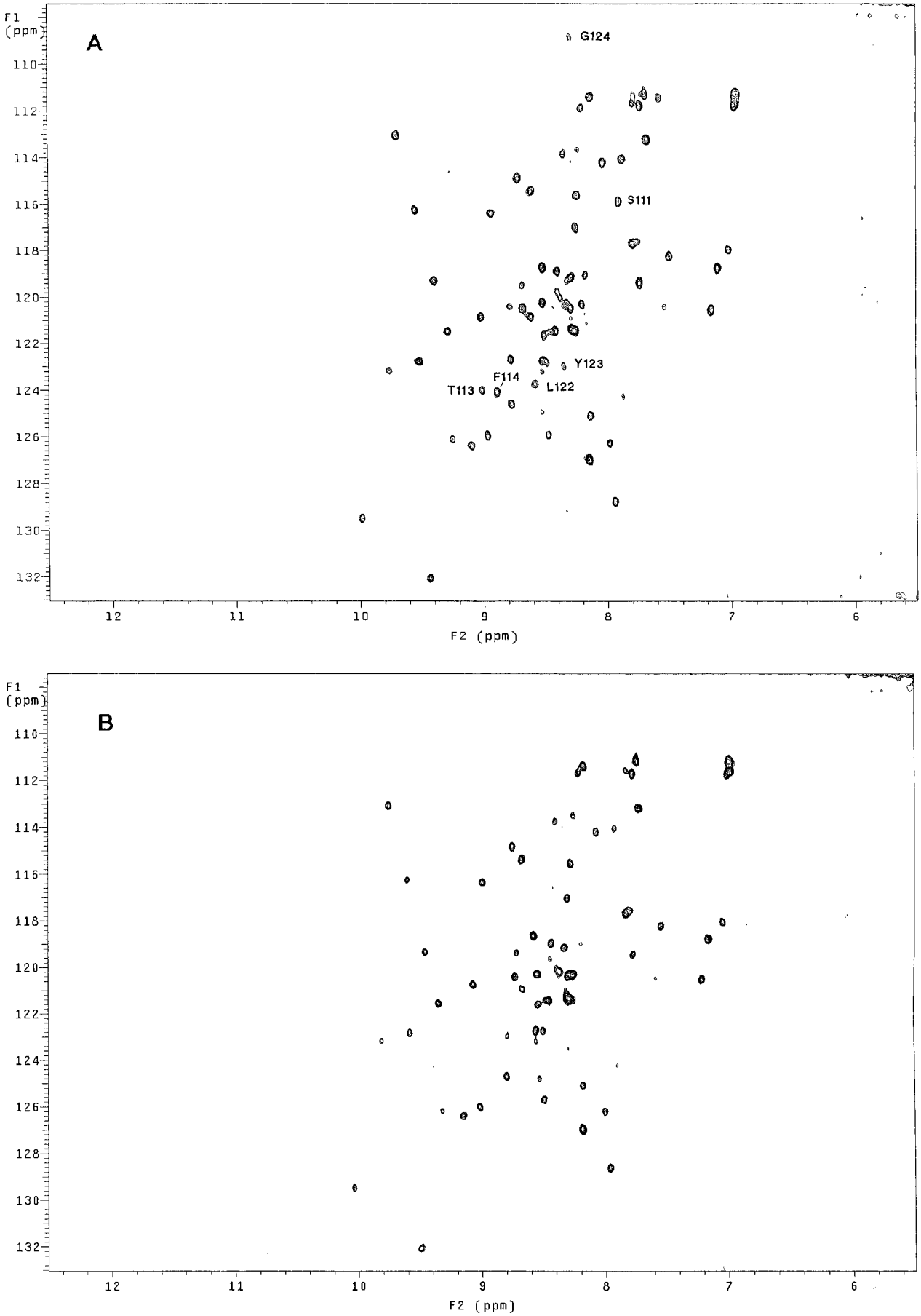

FIGURE 9: Contour plot of the gradient-enhanced ^{15}N HSQC of the Cys2 domain of PKC-γ. The protein concentration was 0.1 mM dissolved in 25% CD_3CN/75% H_2O, with 50 mM KPO_4 and 100 mM KCl (pH 6.7) at 20 °C. The spectral width is 1582.3 Hz (f_1) × 9434.0 Hz (f_2) with 64 (t_1) × 1024 (t_2) complex points. Four scans were taken for each t_1 complex point. The t_1 dimension was linearly predicted to 128 complex points and zero filled to 256 complex points before Fourier transformation (A) before adding phorbol and (B) after adding 0.2 mM phorbol.

backbone (N, C_α, C′) or all heavy atoms in residues 102−151 was 0.50 ± 0.09 and 1.10 ± 0.15 Å, respectively. The rmsd for all the secondary structure and well-defined turns (102−108, 112−122, and 129−147) was 0.33 ± 0.07 Å for backbone and 0.98 ± 0.13 Å for all heavy atoms. A stereoview of the superimposed 30 final structures is shown in Figure 4. Ramachandran plots of the backbone ϕ, ψ angles for the 30 final structures demonstrated that most of the angles are within the energetically favored regions of ϕ, ψ space (Figure 5A). When residues with AOP <0.9 were excluded, the Ramachandran plot improves (Figure 5B).

Description of the Solution Structure. The resulting conformation of the PKC-γ has five β-strands and one α-helix (Figures 6 and 7). They are 102−108 (β A), 113−115 (β B), 120−122 (β C), 129−132 (β D), 137−140 (β E), and 143−147 (α A). There are two type I β-turns defined by the sequential NOEs and ϕ, ψ angles: 116−119 (BC) and 133−136 (DE). Another tight turn is 141−142 (EA). Beside C- and N-terminal residues, loop 123−128 (CD) is the longest and least defined loop, and loop 109−112 (AB) is the second least defined region (Figure 2A,B). The corresponding region of the X-ray structure of PKC-δ has the largest B-factors (Figure 2C) as well. The residues on loops AB (110−112) and CD (123,124) as well as βB (113) and βC (122) comprise the phorbol-binding site (colored yellow in Figures 4 and 7) as demonstrated below. The zinc-binding residues include H102, C132, C135, and C151 for site 1, with H140, C115, C118, and C143 for site 2 (Figure 7). The zinc binding stabilizes these two type I β-turns. These tight turns are well defined and have small rmsd values (Figure 2B).

The Phorbol-Binding Site. Phorbol dibutyrate (PDB) bound tightly, as observed by slow exchange of free and bound resonances, to PKC-γ Cys2 protein, but the complex quickly precipitated in aqueous buffers when lipid micelles were absent. However, PDB and Cys2 protein were found to be cosoluble in 25% CD_3CN/75% H_2O. After titrating PDB into PKC-γ, ^{15}N HSQC spectra were collected to identify which residues were perturbed. Only the signals of residues S111, T113, F114, L122, Y123, and G124 disappeared due to chemical exchange broadening, indicating that these residues are involved in phorbol binding (Figure 9). These residues are colored yellow in Figures 4, 7, and 8. Changing the temperature in the range of 10−40 °C had little effect on the spectrum, where PDB and Cys2 protein were in moderate exchange between free and bound states. This finding is consistent with the X-ray structure of the PKC-δ/phorbol 13-acetate complex. The presence of organic solvent may have reduced the binding affinity of PDB.

Interaction with Lipids. Lipid micelle titrations into PKC-γ were followed by ^{15}N HSQC spectra to identify which residues within the protein were affected. The signals of residues around the phorbol-binding site (106−111, 113−116, L121, 124−127, 130) were broadened. The signals of S120, L122, and Y123, part of the phorbol binding site, were certainly shifted if not broadened. In addition, the signals of the zinc site 2 (C115, C118, 138−145, 147) and two residues on the zinc site 1 (H102, C132) were also broadened. Residues Q128−G129 have little solvent exposure (Figure 2D), and their amide resonances were not affected by the lipids. Protein residues whose amide proton signals were broadened by lipid interaction are colored cyan in Figures 4, 7, and 8. These effects were identical at all lipid compositions tested, provided the overall lipid:protein ratios were >70:1. Including PDB with the lipids had little discernible effect on most of the spectrum. However, the signals of residues H117, G119, and E136 were also broadened, but the signal of residue V147 was recovered when PDB was present (Figure 8B). As shown in Figure 8, only the top half of the molecule, including the phorbol-binding site and zinc-binding site 2, interacted with lipid micelles. Thus, only the top half of the Cys2 domain (cyan in Figure 8) apparently inserts into the lipid micelles.

CONCLUSION

The complete chemical shift assignment of ^{13}C, ^{15}N, and ^{1}H of the Cys2 domain of PKC-γ has been accomplished by heteronuclear multidimensional NMR. The N-terminus (92−99) and C-terminus (154−172) of the Cys2 domain are highly flexible. A well-defined core of the Cys2 domain (100−153) has been determined to high resolution by 4D NOESY and coupling constant measurements. The interaction of PKC-γ with phorbol was monitored by ^{15}N HSQC. The selective broadening of residue signals upon phorbol binding clearly indicates the binding sites for phorbol are residues S111, T113, F114, L122, Y123, and G124. The interactions of lipids with PKC-γ, in the absence or presence of phorbol, were also monitored by ^{15}N HSQC. The exchange broadening of the protein residues that have interaction with lipids are located on half of the well-defined Cys2 domain.

ACKNOWLEDGMENT

We thank Dr. Bennett T. Farmer, II, and Dr. Lewis E. Kay for many useful Varian pulse programs and Dr. Stephan Grzesiek and Dr. Ad Bax for details of the AMNESIA shaped pulse. We also thank Mr. Bruce Wisely for assistance in protein expression and Dr. Lisa Shewchuck and Mr. Derril Willard for advice on purification of the protein. Mass spectral analyses of protein samples were done by Mr. Kevin Blackburn and Mr. Rod Davis, whose services were crucial in optimizing the protein purification protocol. We also thank Dr. Sujoy Ghosh for many helpful discussions.

SUPPORTING INFORMATION AVAILABLE

One table giving a complete list of ^{1}H, ^{13}C, and ^{15}N resonance assignments for the PKC-γ Cys2 domain (9 pages). Ordering information is given on any current masthead page.

REFERENCES

Archer, S. J., Ikura, M., Torchia, D. A., & Bax, A. (1991) *J. Magn. Reson. 95*, 636−641.

Bax, A., & Pochapsky, S. S. (1992) *J. Magn. Reson. 99*, 638−643.

Bax, A., Clore, G. M., & Gronenborn, A. M. (1990a) *J. Magn. Reson. 88*, 425−431.

Bax, A., Clore, G. M., Driscoll, P. C., Gronenborn, A. M., Ikura, M., & Kay, L. E. (1990b) *J. Magn. Reson. 87*, 620−627.

Bax, A., Max, D., & Zax, D. (1992) *J. Am. Chem. Soc. 114*, 6923−6925.

Bell, R. M., & Burns, D. J. (1991) *J. Biol. Chem. 266*, 4661−4664.

Bendall, M. R., & Skinner, T. (1996) *J. Magn. Reson. A* (in press).

Burns, D. J., & Bell, R. M. (1991) *J. Biol. Chem. 266*, 18330−18338.

Clore, G. M., Kay, L. E., Bax, A., & Gronenborn, A. M. (1991) *Biochemistry 30*, 12−18.

Dekker, L. V., & Parker, P. J. (1994) *Trends Biochem. Sci. 19*, 73−77.

Delaglio, F., Grzesiek, S., Vuister, G. W., Zhu, G., Pfeifer, J., & Bax, A. (1995) *J. Biomol. NMR 6*, 277−293.
Fesik, S. W., & Zuiderweg, E. R. P. (1988) *J. Magn. Reson. 78*, 588.
Ghosh, S., Basu, S. S., Strum, J. C., Basu, S., & Bell, R. M. (1995) *Anal. Biochem. 225*, 376−378.
Grzesiek, S., & Bax, A. (1992) *J. Am. Chem. Soc. 114*, 6291−6293.
Grzesiek, S., & Bax, A. (1993a) *J. Biomol. NMR 3*, 185−204.
Grzesiek, S., & Bax, A. (1993b) *J. Biomol. NMR 3*, 627−638.
Grzesiek, S., & Bax, A. (1995) *J. Am. Chem. Soc. 117*, 6527−6531.
Grzesiek, S., Ikura, M., Clore, G. M., Gronenborn, A. M., & Bax, A. (1992) *J. Magn. Reson. 96*, 215−221.
Grzesiek, S., Anglister, J., & Bax, A. (1993a) *J. Magn. Reson. B 101*, 114−119.
Grzesiek, S., Vuister, G. W., & Bax, A. (1993b) *J. Biomol. NMR 3*, 487−493.
Hommel, U., Zurini, M., & Luyten, M. (1994) *Nat. Struct. Biol. 1*, 383−387.
Ichikawa, S., Hatanaka, H., Takeuchi, Y., Ohno, S., & Inagaki, F. (1995) *J. Biochem. 117*, 566−574.
Kabsch, W. (1976) *Acta Crystallogr. A32*, 922−923.
Kay, L. E., & Bax, A. (1990) *J. Magn. Reson. 86*, 110−126.
Kay, L. E., Keifer, P., & Saarinen, T. (1992) *J. Am. Chem. Soc. 114*, 10063−10065.
Kay, L. E., Xu, G. Y., & Yamazaki, T. (1994) *J. Magn. Reson. A 109*, 129−133.
Kazanietz, M. G., Wang, S., Milne, G. W. A., Lewin, N. E., Liu, H. L., & Blumberg, P. M. (1995) *J. Biol. Chem. 270*, 21852−21859.
Kraulis, P. (1991) *J. Appl. Crystallogr. 24*, 946−950.
Lee, M. H., & Bell, R. M. (1989) *J. Biol. Chem. 264*, 14797−14805.
Logan, T. M., Olejniczak, E. T., Xu, R. X., & Fesik, S. W. (1992) *FEBS Lett. 314*, 413−418.
Logan, T. M., Olejniczak, E. T., Xu, R. X., & Fesik, S. W. (1993) *J. Biomol. NMR 3*, 225−231.
Marion, D., Driscoll, P. C., Kay, L. E., Wingfield, P. T., Bax, A., Gronenborn, A. M., & Clore, G. M. (1989) *Biochemistry 28*, 6150−6156.
Martigny-Baron, G., Kazanietz, M. G., Mischak, H., Blumberg, P. M., Kochs, G., Hug, H., Marme, D., & Schachtele, C. (1993) *J. Biol. Chem. 268*, 9194−9197.
Meadows, R. P., Netteshiem, D. G., Xu, R. X., Olejniczak, E. T., Petros, A. M., Holzman, T. F., Severin, J., Gubbins, E., Smith, H., & Fesik, S. W. (1993) *Biochemistry 32*, 754−765.
Muhandiram, D. R., & Kay, L. E. (1994) *J. Magn. Reson. B 103*, 203−216.
Muhandiram, D. R., Farrow, N. A., Xu, G.-Y., Smallcombe, S. H., & Kay, L. E. (1993) *J. Magn. Reson. B 102*, 317−321.
Newton, A. C. (1993) *Annu. Rev. Biophys. Biomol. Struct. 22*, 1−25.
Nishizuka, Y. (1984) *Science 225*, 1365−1370.
Nishizuka, Y. (1992) *Science 258*, 607−614.
Nishizuka, Y. (1995) *FASEB J. 9*, 484−496.
Ohno, Y., Fujii, T., Igarashi, K., Kuno, T., Tanaka, C., Kikkawa, U., & Nishizuka, Y. (1989) *Proc. Natl. Acad. Sci. U.S.A. 86*, 4868−4871.
Olejniczak, E. T., Xu, R. X., & Fesik, S. W. (1992) *J. Biomol. NMR 2*, 655−659.
Quest, A. F. G., Bardes, E. S. G., & Bell, R. M. (1994a) *J. Biol. Chem. 269*, 2953−2960.
Quest, A. F. G., Bardes, E. S. G., & Bell, R. M. (1994b) *J. Biol. Chem. 269*, 2961−2970.
Rando, R. R., & Kishi, Y. (1992) *Biochemistry 31*, 2211−2218.
Schussheim, A. E., & Cowburn, D. (1987) *J. Magn. Reson. 71*, 371−378.
Sharkey, N. A., Leach, K. L., & Blumberg, P. M. (1984) *Proc. Natl. Acad. Sci. U.S.A. 81*, 607−610.
Silver, M. S., Joseph, R. I., & Hoult, D. I. (1984) *Phys. Rev. A 31*, 2753.
Slater, S. J., Ho, C., Kelly, M. B., Larkin, J. D., Taddeo, F. J., Yeager, M. D., & Stubbs, C. D. (1996) *J. Biol. Chem. 271*, 4627−4631.
Toullec, D., Pianetti, P., Coste, H., Bellevergue, P., Grand-Perret, T., Ajakane, M., Baudet, V., Boissin, P., Boursier, E., Loriolle, F., Duhamel, L., Charon, D., & Kirilovsky, J. (1991) *J. Biol. Chem. 266*, 15771−15781.
Vuister, G. W., & Bax, A. (1993a) *J. Am. Chem. Soc. 115*, 7772−7777.
Vuister, G. W., & Bax, A. (1993b) *J. Magn. Reson. B 102*, 228−231.
Vuister, G. W., Wang, A., & Bax, A. (1993a) *J. Am. Chem. Soc. 115*, 5334.
Vuister, G. W., Clore, G. M., Gronenborn, A. M., Powers, R., Garrett, D. S., Tschudin, R., & Bax, A. (1993b) *J. Magn. Reson. B 101*, 210−213.
Wang, S., Milne, G. W. A., Nicklaus, M. C., Marquez, V. E., Lee, J., & Blumberg, P. M. (1994a) *J. Med. Chem. 37*, 1326−1338.
Wang, S., Zaharevitz, D. W., Sharma, R., Marquez, V. E., Lewin, N. E., Du, L., Blumberg, P. M., & Milne, G. W. A. (1994b) *J. Med. Chem. 37*, 4479−4489.
Weinstein, I. B. (1988) *Cancer Res. 48*, 4135−4143.
Wittekind, M., & Muller, L. (1993) *J. Magn. Reson. B 101*, 201−205.
Wuthrich, K. (1986) *NMR of Proteins and Nuclear Acids*, John Wiley & Sons, New York.
Xia, T.-H. (1996) Poster at XVIIth ICMRBS, Keystone, CO.
Yamazaki, T., Forman-Kay, J. D., & Kay, L. E. (1993) *J. Am. Chem. Soc. 115*, 11054−11055.
Zhang, O., Kay, L. E., Olivier, J. P., & Forman-Kay, J. D. (1994) *J. Biomol. NMR 4*, 845−858.
Zhang, G., Kazanietz, M. G., Blumberg, P. M., & Hurley, J. H. (1995) *Cell 81*, 917−924.
Zhu, G., & Bax, A. (1990) *J. Magn. Reson. 90*, 405−410.
Zhu, G., & Bax, A. (1992) *J. Magn. Reson. 100*, 202−207.

BI970833A